Low Driving Voltage Band-filling-based III-V-on-Silicon Electroabsorption Modulator

Qiangsheng Huang,[1,2] Yingchen Wu,[2,3] Keqi Ma,[1] Jianhao Zhang,[1] Weiqiang Xie,[2] Xin Fu,[1,2] Yaocheng Shi,[1] Jianxin Cheng,[4] Kaixuan Zhang,[4] Chenzhao Zhang,[4] Jianjun He,[3] Dries Van Thourhout,[2] Gunther Roelkens,[2] Liu Liu,[4] and Sailing He[1,4,a)]

[1)]Centre for Optical and Electromagnetic Research, Zhejiang Provincial Key Laboratory for Sensing Technologies, Zhejiang University, Hangzhou, 310058, China
[2)]Photonics Research Group, Department of Information Technology, Ghent University-IMEC, Ghent B-9000, Belgium
[3)]State Key Laboratory of Modern Optical Instrumentation, Centre for Integrated Optoelectronics, Department of Optical Engineering, Zhejiang University, Hangzhou, China 310027
[4)]ZJU-SCNU Joint Research Center of Photonics, Centre for Optical and Electromagnetic Research, South China Academy of Advanced Optoelectronics, Science Building No.5, South China Normal University, Higher-Education Mega-Center, Guangzhou 510006, China

(Dated: 15 January 2016)

In this paper, a new method for realizing a low driving voltage electroabsorption modulator based on the band-filling effect is demonstrated. The InP-based electroabsorption modulator is integrated using DVS-BCB adhesive bonding on a silicon-oninsulator waveguide platform. When the electroabsorption modulator is forward biased, the band-filling effect occurs, which leads to a blue shift of the exciton absorption spectrum while the absorption strength stays almost constant. In static operation, an extinction ratio of more than 20dB with 100mV bias variation is obtained in an 80 m long device. In dynamic operation, 1.25Gbps modulation with a 6.3dB extinction ratio is obtained using only a 50mV peak-to-peak driving voltage. The band-filling effect provides a novel method for realizing ultra-low-driving-voltage electroabsorption modulators.

Quantum-confined Stark effect (QCSE) based electroabsorption modulators (EAM) have high speed, low energy consumption, relatively high extinction ratio and small footprint.[1,2] These features make EAMs widely used in optical communication. In addition, EAMs can also be used as high speed photodetectors.[3] This dual function property makes EAMs advantageous in on-chip optical transceivers[4] and compact optoelectronic oscillators (OEO).[5] Recently, silicon photonics integrated with electronic devices fabricated in CMOS production lines has become an enabling technology for the realization of integrated optical systems.[6,7] High speed InP-based EAMs have also been successfully implemented in silicon photonic circuits though hybrid bonding technology.[1,4,8,9] However, an EAM directly driven by the low voltage swing signal from an advanced digital logical CMOS driver is still missing. Recently, a sub-100 mV driving voltage silicon modulator based on the tuning of the resonant wavelength in a high Q microring resonator and photonic crystal cavity has been demonstrated.[10,11] However, those devices are very sensitive to fabrication imperfections and cannot be used as photodetectors. For EAMs based on QCSE, it is challenging to reduce the driving voltage without an increase in the modulator size and insertion loss. Even when using a complex slow-light Bragg waveguide to enhance light-matter interaction, it is still hard to reduce the driving voltage below 100 mV and integrate with silicon photonics.[12] Therefore, it is desirable to find a new, simple way to reduce the driving voltage without requiring complex fabrication procedures.

The band-filling effect in modulation-doped MQWs has been studied in the 1980s.[13] The band-filling effect, in which the conduction subbands are filled with a two-dimensional (2D) electron gas, results in a blue shift of the absorption edge. By controlling the bias voltage, electron concentrations in the MQWs region can be adjusted. In this way, the MQW absorption edge can be controlled by bias voltage through the band-filling effect. This effect has been used in 100 mV driven active Q-switching lasers using modulation-doped quantum well.[14] However, there is still a lack of an EAM based on the band-filling effect.

In this paper, we demonstrate a new type low driving voltage EAM based on the band-filling effect at 1.55 μm. The EAM is bonded on and coupled to a silicon-on-insulator (SOI) waveguide circuit, which makes it attractive for direct digital CMOS drive.

Fig. 1 shows the cross-section view of the EAM integrated on SOI using DVS-BCB adhesive bonding technology.[8] It consists of a silicon ridge waveguide, a thin bonding layer and a III-V p-i-n structure. The 380 nm thick silicon ridge waveguide is etched 160 nm deep and planarized using SiO2. The thin bonding layer includes a 30 nm thick DVS-BCB layer and 15 nm SiO2. At the top of the III-V p-i-n structure, there is a 100nm p-InGaAs (1.5×10^{19} cm^{-3}) layer connected with the signal metal line. Below it, there is a 1.5 μm gradually-doped (2×10^{18} to $1 \times 10 \times^{18}$ cm^{-3}) p-InP. In the intrinsic region, a multiple-quantum-well (MQW) stack is sandwiched between two separate confinement heterostructure layers of In$_{0.52}$Al$_{0.16}$Ga$_{0.32}$As. The MQW stack
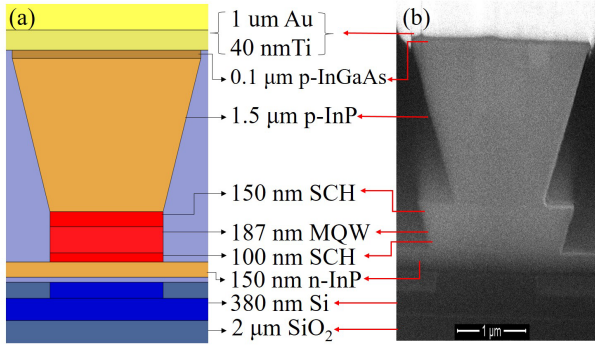
[a)]Electronic mail: sailing@kth.se

FIG. 1. (a) Cross-section view of the EAM bonded on SOI. (b) SEM image of the cross-section of the fabricated III-V/Si hybrid waveguide.
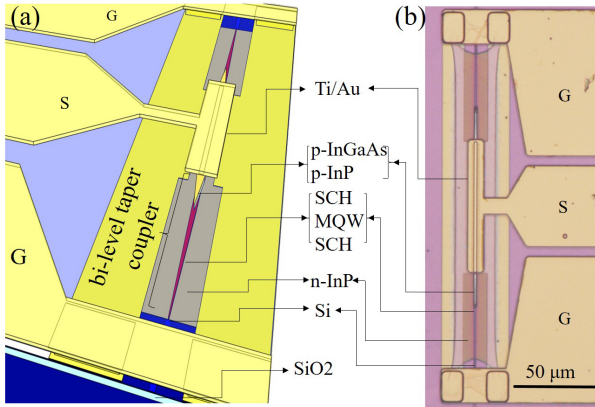

FIG. 2. (a) Three-dimensional sketch of the EAM bonded on SOI. (b) Top microscope image of the III-V/Si hybrid integrated EAM.

(photoabsorption edge at 1560 nm) consists of 10 compressively strained $In_{0.65}Al_{0.09}Ga_{0.26}As$ quantum wells and 11 tensile strained $In_{0.42}Al_{0.17}Ga_{0.39}As$ barriers. At the bottom of the III-V structure, a 150 nm thin n-InP (3×10^{18} cm^{-3}) layer is connected with the ground metal lines. The detailed epitaxial layer structure is shown in Fig. 1(a) and (b).

The fabrication process of this EAM is simpler than that of our previous laser/modulator.[4,8,9] Thanks to the highly selective wet etching process used, a photoresist mask instead of a SiN hard mask can be used to define the III-V waveguide. In this way, the deposition and etching of SiN hardmask layers by PECVD and ICP-RIE respectively is avoided. The SOI waveguide circuit is fabricated through an ePIXfab Multi Project Wafer run.[15] The silicon ridge waveguide is 1.5 μm wide. After bonding and removing the InP substrate, the InGaAs layer is patterned by wet-etching ($H_3PO_4:H_2O_2:H_2O = 1:1:20$) using a photoresist mask. Then the p-InP waveguide is defined using the InGaAs pattern as a mask through wet etching ($HCl:H_2O = 1:1$). The waveguide cross section becomes an inverted trapezoid with a width of 2.5 μm at

the top and 1.5 μm at the bottom. The intrinsic layer is patterned using a 5 μm wide photoresist mask. By under-etching the intrinsic region ($Citric:H_2O_2 = 20:1$) its width is reduced to 1.5 μm. A 0.1 μm thick Ni/Ge/Au alloy is deposited onto the n-InP for n-contacts. Then the n-InP is wet etched ($HCl:H_2O = 1:1$) in order to isolate the devices. A 2.5 μm thick DVS-BCB is used for passivation and planarization. Via holes are formed in the DVS-BCB for metal connection. 40 nm / 1 m thick Ti/Au is deposited onto the p-InGaAs and n-contacts for the 100 μm pitch ground-signal-ground (GSG) metal contact. Fig. 2(a) shows the three-dimensional view of the designed lumped electrode EAM. Fig.1(b) shows the cross section of the fabricated III-V/Si hybrid waveguide structure. Fig. 2(a) shows a schematic view of the complete device. Fig. 2(b) shows a top-down photograph of the fabricated lumped electrode EAM.

The optical confinement factor in the multi-quantum well stack is around 24%. The mode conversion from the silicon ridge waveguide to the EAM waveguide is achieved by a 45 μm long bi-level taper.[9,16] The silicon ridge waveguide remains 1.5 μm wide in the bi-level taper. In the first part of the taper, the mode is converted from the silicon ridge waveguide mode that of the hybrid structure with a III-V waveguide without the thick p-InP layer, with the intrinsic layer width laterally tapered from 0.2 μm to 1.5 μm. The second part of the taper transforms the optical mode into the full III-V waveguide mode, with the p-InP layer laterally tapered from 0.2 μm to 2.5 μm and the intrinsic layer kept 1.5 μm wide. The simulated coupling efficiency between the silicon ridge waveguide and EAM waveguide is around 98%.

The EAM with InAlGaAs quantum wells has a strong exciton absorption peak at the absorption edge due to its large conduction band offset.[2] Since the band-to-band continuum transition energy (which is above the exciton transition energy) has a small influence on the absorption edge, we adopt a theoretical model only containing the exciton transition, in order to simplify calculation of the absorption spectra and the shift of the absorption edge for the EAM.[17] The material parameters of the MQW structure, such as the effective electron/hole mass, Luttinger parameters, band energy levels, etc., are taken from Ref. 18, according to the composition of each layer. The half-linewidth for the absorption peak varies from 1 meV at zero electric field to 1.4 meV at 42 KV/cm. The effective mass m* of the average matrix element is 0.0064 m$_0$,[17] where m$_0$ is the electron mass.

The simulated exciton absorption spectra for the 80 m long EAM are shown in Fig. 3. Due to the p-i-n structure, there is a built-in electric field at 0 V. The zero electric field in the intrinsic layer is achieved at a forward bias of 0.6 V. Below 0.6 V, the EAM absorption spectra for the EAM are calculated based on QCSE. The exciton absorption peak red shifts with increasing applied electric field. Due to the decreasing electron-hole overlap integral with increasing electric field, the absorption magnitude decreases. Above 0.6V, the absorption spectra for the
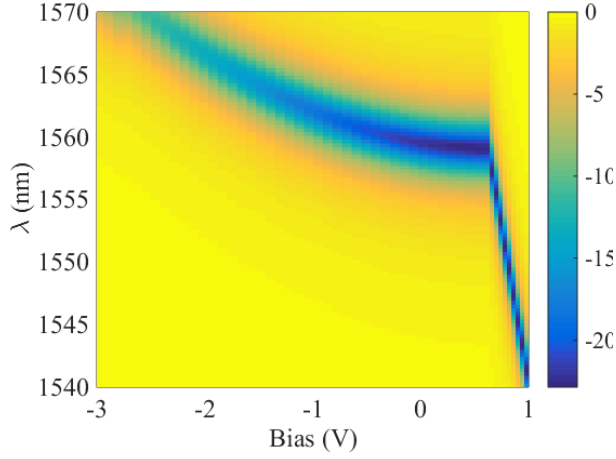
FIG. 3. The simulated exciton absorption spectra (dB) for the 80 μm long EAM with different bias voltages. The strongest absorption is more than 20dB.

FIG. 4. (a) The bias dependent normalized transmission for the 80 μm long EAM at 1.55 μm. (b) The exciton absorption spectra (dB) for different bias voltages. The strongest absorption is more than 20 dB.

EAM are calculated based on the band-filling effect. The exciton absorption peak blue shifts with current injected into the conduction band. Because the electron-hole overlap integral remains almost constant with increase in current density, the absorption does not decrease in magnitude. The exciton transition energy shift ΔE is given by: $\Delta E = (1 + m_e/m_h)E_F$, where E_F is the Fermi energy level, and m_e and m_h are the effective electron and hole mass, respectively.[13] When E_F is substantially higher than the lowest conduction subbands E_1, E_F is linear with carrier density in the quantum well.[19] Because the carrier density is proportional to the injected current, and the injected current is directly related to the applied voltage, the absorption peak shift is directly proportional with the applied voltage. In this way, by modulating the applied voltage, we can modulate the absorption.

We first measure the EAMs static performance as a function of bias at 1.55 μm, shown in Fig. 4(a). The measurement results are normalized to a straight waveguide using the same fiber-chip interface. The insertion loss of the EAM is around 5 dB, larger than the simulation results. This is attributed to the fact that the width of the intrinsic region in the fabricated device is larger than the designed value of 1.5 μm, shown in Fig. 1(b). In this case, the bi-level taper coupler will excite higher order modes and cause unwanted reflection during mode transformation, especially in the first level taper.[16] Fig. 4(a) shows that there are two regimes of absorption variation versus bias voltage. In the reverse bias, the absorption variation is caused by continuum transition absorption. The extinction ratio is around 4dB with the voltage changing from -1V to -2V. In the forward bias, the absorption variation is caused by exciton transition absorption. The change in absorption is more than 20 dB with only 100 mV bias variation. The measured absorption spectra with bias variation are shown in Fig. 4(b). The exciton peak absorption and shifts are in good agreement with the simulation results shown in Fig. 3. In the forward
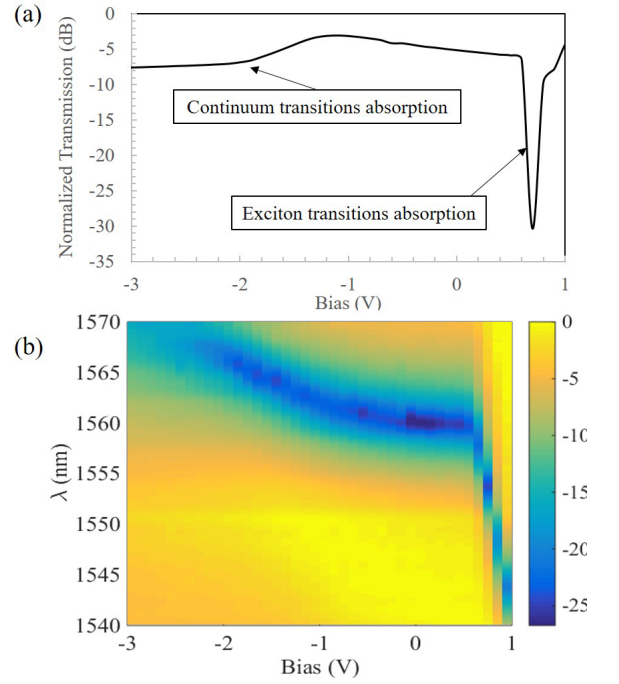
bias, the blue shift rate of the exciton absorption peak is around 50 nm/V, without a reduction in absorption strength. Therefore, a low driving voltage EAM can be realized in the forward bias.

Next, we measure the high-speed performance of the EAM at 1.55 μm. A non-return-to-zero (NRZ) 2^{31}-1 pseudorandom bit sequence (PRBS) pattern is generated and attenuated to a level of 50 mV swing, and then applied to the III-V-on-silicon EAM via a bias-T providing a forward bias of 0.6 V. The modulated light is coupled out to a fiber through a fiber-to-chip grating coupler and amplified by an erbium-doped fiber amplifier (EDFA). The amplified spontaneous emission caused by the EDFA is filtered out by a narrow optical filter. Eye diagrams are measured using a Tektronix 8300A digital series analyzer. The 1.25 Gbps eye diagram of the EAM is shown in Fig. 5(a). The dynamic extinction ratio is 6.3 dB, which is twice as large as the low voltage drive silicon modulators based on tuning the resonant wavelength with the same peak-to-peak voltage.[11] The method to calculate the energy consumption for the EAM is presented in Ref. 1. Because the cross-section of our 80 μm long EAM is the same as our previous 100 μm long modulator,[9] the junction capacitance is estimated to be around 116 fF. The transient energy consumption for this EAM is 0.29 fJ/bit. The transient energy consumption can be further reduced by narrowing the intrinsic layer width to decrease the junction capacitance. The DC energy consumption per bit at 1.25 Gbps is 110 fJ/bit, which can
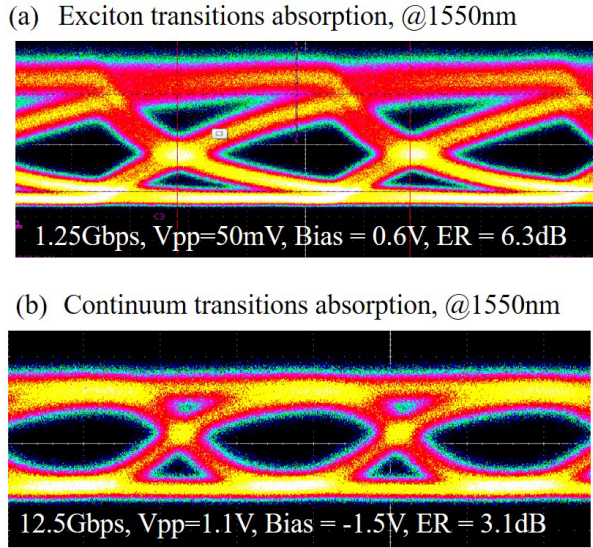
(a) Exciton transitions absorption, @1550nm

1.25Gbps, Vpp=50mV, Bias = 0.6V, ER = 6.3dB

(b) Continuum transitions absorption, @1550nm

12.5Gbps, Vpp=1.1V, Bias = -1.5V, ER = 3.1dB

FIG. 5. Measured 2^{31}-1 PRBS NRZ eye diagrams at 1.55 μm (a) 1.25 Gbps at forward bias 0.6 V. (b) 12.5 Gbps at reverse bias -1.5 V.

be reduced by increasing the modulator speed.

Fig. 5(b) shows the high-speed performance for the same EAM at reverse bias. The speed of the EAM with a lumped electrode working under reverse bias is limited by the RC time constant.[1,9] However, for the EAM working under forward bias, the rise and fall time is limited by the carrier lifetime in the MQWs. However, using modulation-doped MQWs to move the Fermi energy level above the lowest confined state in the conduction band at zero bias, we can shift the work point to reverse bias.[13,14] In this way, carrier lifetime can be reduced thereby increasing the band-filling based EAM modulation bandwidth.

In summary, we have demonstrated a III-V-on-silicon electroabsorption modulator based on the band filling effect. The coupling to a silicon waveguide is achieved through a bi-level taper coupler. With 100 mV bias variation, the DC extinction ratio can be adjusted more than 20 dB. The exciton absorption peak shifts and intensity variation are in good agreement with the simulation results. A clear open eye diagram is obtained at 1.25 Gbps with a dynamic extinction ratio of 6.3 dB. The peak-to-peak driving voltage is only 50 mV. The speed of the present device is limited by carrier lifetime and can be further improved by using modulation-doped multi-quantum wells. The insertion loss and transient energy consumption can be further improved with optimized fabrication processes.

ACKNOWLEDGMENTS

[1]Y. Tang, J. D. Peters, and J. E. Bowers, IEEE Photonic Tech L **24**, 1689 (2012).

[2]H. Fukano, T. Yamanaka, M. Tamura, and T. Kondo, J LIGHTWAVE TECHNOL **24**, 2219 (2006).

[3]R. B. Welstand, S. A. Pappert, C. K. Sun, J. T. Zhu, Y. Z. Liu, and P. K. L. Yu, IEEE Photonic Tech L **8**, 1540 (1996).

[4]K. Chen, Q. Huang, J. Zhang, J. Cheng, X. Fu, C. Zhang, K. Ma, Y. Shi, D. V. Thourhout, G. Roelkens, L. Liu, and S. He, "Wavelength-multiplexed duplex transceiver based on IIIV/Si hybrid integration for off-chip and on-chip optical interconnects," IEEE Photon. J. (accepted for publication).

[5]P. Zhou, S. Pan, D. Zhu, R. Guo, F. Zhang, and Y. Zhao, IEEE Photonic Tech L **26**, 1041 (2014).

[6]D. Marpaung, C. Roeloffzen, R. Heideman, A. Leinse, S. Sales, and J. Capmany, Laser Photonics Rev. **7**, 506 (2013).

[7]C. Sun, M. T. Wade, Y. Lee, J. S. Orcutt, L. Alloatti, M. S. Georgas, A. S. Waterman, J. M. Shainline, R. R. Avizienis, S. Lin, B. R. Moss, R. Kumar, F. Pavanello, A. H. Atabaki, H. M. Cook, A. J. Ou, J. C. Leu, Y. Chen, K. Asanovi, R. J. Ram, M. A. Popovi, and V. M. Stojanovi, Nature **528**, 534 (2015).

[8]G. Roelkens, A. Abassi, P. Cardile, U. Dave, A. de Groote, Y. de Koninck, S. Dhoore, X. Fu, A. Gassenq, N. Hattasan, Q. Huang, S. Kumari, S. Keyvaninia, B. Kuyken, L. Li, P. Mechet, M. Muneeb, D. Sanchez, H. Shao, T. Spuesens, A. Z. Subramanian, S. Uvin, M. Tassaert, K. van Gasse, J. Verbist, R. Wang, Z. Wang, J. Zhang, J. van Campenhout, X. Yin, J. Bauwelinck, G. Morthier, R. Baets, and D. van Thourhout, Photonics **2**, 969 (2015).

[9]X. Fu, J. Cheng, Q. Huang, Y. Hu, W. Xie, M. Tassaert, J. Verbist, K. Ma, J. Zhang, K. Chen, C. Zhang, Y. Shi, J. Bauwelinck, G. Roelkens, L. Liu, and S. He, Optics Express **23**, 18686 (2015).

[10]S. Manipatruni, K. Preston, L. Chen, and M. Lipson, Optics Express **18**, 18235 (2010).

[11]A. Shakoor, K. Nozaki, E. Kuramochi, K. Nishiguchi, A. Shinya, and M. Notomi, in *Advanced Photonics for Communications* (Optical Society of America, San Diego, California United States, 2014) p. IW3A.6.

[12]X. Gu, S. Shimizu, T. Shimada, A. Matsutani, and F. Koyama, Applied Physics Letters **102**, 031118 (2013).

[13]G. Livescu, D. A. Miller, D. Chemla, M. Ramaswamy, T. Chang, N. Sauer, A. Gossard, and J. English, IEEE J Quantum Electron **24**, 1677 (1988).

[14]V. Kalinovsky, T. Shubina, I. Y. Shvechikov, and A. Toropov, J PHYS III **3**, 1021 (1993).

[15]See http://www.epixfab.eu/ for more information about ePIXfab Multi Project Wafer run; accessed 5 Jan. 2015. (last accessed 15 Jan. 2016).

[16]Q. Huang, J. Cheng, L. Liu, Y. Tang, and S. He, Applied optics **54**, 4327 (2015).

[17]P. J. Mares and S. L. Chuang, Journal of Applied Physics **74**, 1388 (1993).

[18]E. H. Li, Physica E: Low-dimensional systems and Nanostructures **5**, 215 (2000).

[19]L. A. Coldren and S. W. Corzine, "Diode lasers and photonic integrated circuits," (John Wiley & Sons, Inc., New York, 1995) Chap. 7, pp. 415–416, 1st ed.